ELSEVIER

Chemical Engineering Science 60 (2005) 1603–1617

Chemical Engineering Science

www.elsevier.com/locate/ces

Dynamics and control of thin film surface microstructure in a complex deposition process

Dong Ni, Panagiotis D. Christofides*

Department of Chemical Engineering, University of California, 5531 Boelter Hall, Box 951592, Los Angeles, CA 90095-1592, USA

Received 5 January 2004; received in revised form 8 October 2004

Abstract

In this work, a complex deposition process, which includes two types of macromolecules whose growth behaviors are very different, is investigated. This deposition process is influenced by both short- and long-range interactions. The study of this process is motivated by recent experimental results on the growth of high-κ dielectric thin films using plasma-enhanced chemical vapor deposition. A multi-component kinetic Monte-Carlo (kMC) model is developed for the deposition. Both single- and multi-component cases are simulated and the dependence of the surface microstructure of the thin film, such as island size and surface roughness, on substrate temperature and gas phase composition is studied. The surface morphology is found to be strongly influenced by these two factors and growth regimes governed by short- and long-range interactions are observed. Furthermore, two kMC model-based feedback control schemes which use the substrate temperature to control the final surface roughness of the thin film are proposed. The closed-loop simulation results demonstrate that robust deposition with controlled thin film surface roughness can be achieved under a kMC estimator-based proportional integral (PI) feedback controller in the short-range interaction dominated growth regime, while a kMC model-predictive controller is needed to control the surface roughness in the long-range interaction dominated growth regime.

Keywords: Thin film deposition; Feedback control; Complex dynamics; Kinetic Monte-Carlo simulation; Model-predictive control; Long-range interaction; Short-range interaction

1. Introduction

The industrial demands for advanced materials having desirable properties, have driven the development of thin film technology. Today, thin films are used in a wide range of applications, e.g., microelectronic devices, optics, micro-electro-mechanical systems (MEMS) and biomedical products. Various deposition methods, such as physical vapor deposition (PVD) and chemical vapor deposition (CVD), have been developed and widely used to prepare thin films. However, the dependence of the thin film properties, such as spatial uniformity, composition and microstructure, on the deposition conditions, is a severe constraint on reproducing the performance of the thin film. Therefore, in order to meet the stringent requirements on the quality of thin films, real-time feedback control of thin film deposition becomes increasingly important.

Significant research efforts have been made on the feedback control of thin film deposition processes with emphasis on control of film spatial uniformity in rapid thermal processing (RTP) (Baker and Christofides, 1999; Theodoropoulou et al., 1999; Christofides, 2001) and plasma-enhanced chemical vapor deposition (PECVD) (Armaou and Christofides, 1999). In addition to achieving spatially uniform deposition of thin films, one would like to regulate film properties such as microstructure (Lou and Christofides, 2003a, 2005a,b,c) and composition (Ni et al., 2004) that characterize film quality. While deposition uniformity control can be accomplished on the basis of continuum

* Corresponding author. Tel.: +1 310 794 1015; fax: +1 310 206 4107.
E-mail address: pdc@seas.ucla.edu (P.D. Christofides).

0009-2509/$ - see front matter © 2004 Elsevier Ltd. All rights reserved.
doi:10.1016/j.ces.2004.11.005

type distributed models, precise control of film properties requires models that predict how the film state (microscopic scale) is affected by changes in the controllable process parameters (macroscopic scale). This need has motivated extensive research on the development of fundamental mathematical models describing thin film growth.

Kinetic Monte-Carlo (kMC) simulation provides a framework for modelling the effect of macroscopic process variables on the thin film microstructure and has been widely used to simulate CVD processes (see Battaile and Srolovitz (2002) for a review of kMC simulation of CVD). However, the majority of these works have focused on studying the growth kinetics or interface structure while only a few works (Vlachos, 1997; Reese et al., 2001) have addressed the computational efficiency which strongly affects the use of such kMC models within real-time feedback control systems. Recently, a methodology for feedback control of thin film growth using kMC models was developed by Lou and Christofides (2003a,b). The methodology leads to the design of (a) real-time roughness estimators by using multiple small lattice kMC simulators, adaptive filters and measurement error compensators and (b) feedback controllers based on the real-time roughness estimates. The method was successfully applied to control surface roughness in a GaAs deposition process using an experimentally determined kMC process model (Lou and Christofides, 2005a). Other approaches have also been developed to: (a) identify linear deterministic models from outputs of kMC simulators and perform controller design by using linear control theory (Siettos et al., 2003; Armaou et al., 2004), (b) construct reduced-order approximations of the master equation (Gallivan and Murray, 2004), and (c) construct stochastic partial differential equation models using kMC simulations (Ni and Christofides, 2005a,b).

However, among these computationally attractive models, most of them consider only single component systems, and long-range interactions have not been modelled explicitly. In reality, most CVD processes are heterogeneous deposition processes where more than one species participate in the film growth. Moreover, direct long-range interactions (Einstein, 1996) and substrate-mediated long-range interactions (Merrick et al., 2003) are very important in many of these processes. For example, in the PECVD ZrO_2 process, there is a large number of different species present in the gas phase during the deposition, and many of them participate in the thin film growth, particularly, zirconium hydroxide and hydrocarbon species (see Cho et al. (2002) for detailed experimental results). Moreover, recent experimental results (Cho et al., 2003) have shown that, when zirconium hydroxides are the dominant species in the gas phase, the deposited ZrO_2 thin film has a very smooth surface with a roughness value less than half ZrO_2 monolayer, which suggests that the zirconium hydroxide species tend to uniformly cover the substrate surface. On the other hand, when hydrocarbons dominate the gas phase, the deposited ZrO_2 thin film has a very rough surface characterized by big islands, which suggests that the aggregation of the hydrocarbon species on the substrate surface, as a result of long-range interactions, is quite significant. It is quite obvious that a single component kMC model considering only short-range interactions is inadequate to describe the thin film growth in this process. Therefore, a computationally efficient kMC model of heterogeneous deposition processes in which long-range interactions are accounted for is needed.

In this work, a complex deposition process, which includes two types of macromolecules whose growth behaviors are very different, is investigated. This deposition process is influenced by both short- and long-range interactions. The study of this process is motivated by recent experimental results on the growth of high-κ dielectric thin films using plasma-enhanced chemical vapor deposition (PECVD). A multi-component kMC model is developed for the deposition. Both single- and multi-component cases are simulated and the dependence of the surface microstructure of the thin film, such as island size and surface roughness, on substrate temperature and gas phase composition are studied. The surface morphology is found to be strongly influenced by these two factors and growth regimes governed by short- and long-range interactions are observed. Furthermore, two kMC model-based feedback control schemes which use the substrate temperature to control the final surface roughness of the thin film are proposed. The closed-loop simulation results demonstrate that robust deposition with controlled thin film surface roughness can be achieved under a kMC estimator-based proportional integral (PI) feedback controller in the short-range interaction dominated growth regime, while a kMC model-predictive controller is needed to control the surface roughness in the long-range interaction dominated growth regime.

2. Surface microstructure model for thin film growth

Deposition processes such as PECVD, often involve large numbers of participating species with heterogeneous growth behaviors. Here, we study a heterogeneous deposition process in which two types of macromolecules of very different growth behavior, type *A* and type *B*, are present. Type *A* macromolecule is significantly affected by long-range attractions and tends to aggregate with other *A* macromolecules into clusters, i.e., it favors Volmer-Weber (VW) growth mode (Gilmer et al., 1998). Hydrocarbon molecules generated from the decomposition of metal-organic (MO) precursors in a PECVD process are good examples of such type. Type *B* macromolecule favors surface sites of local minimum height, which usually results in Frank-van der Merwe (FM) type of film growth (Gilmer et al., 1998). Metal oxides or hydroxides originated from the MO precursors may behave similar to macromolecules of type *B* as discussed in the introduction.

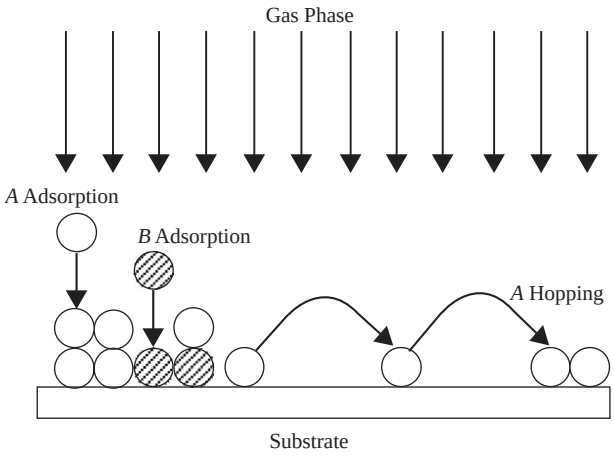

Fig. 1. Thin film growth process.

The geometry of the deposition process is shown in Fig. 1. The gas flux is perpendicular to the substrate surface. Flux compositions, i.e., flux of *A* and *B*, in terms of the number of macromolecules encountered per unit time per surface site, are taken as macroscopic process parameters. They can be measured directly (via mass spectrometer for example) or determined based on the measurements of the partial pressures for each species and gas phase temperature using kinetic theory (Lam and Vlachos, 2001). Thus, we model only the microprocesses taking place on the substrate surface. Both *A* and *B* can diffuse from the gas phase onto the substrate, however, *B* type macromolecules settle to surface sites of local minimum height (surface relaxation) simultaneously during adsorption. Surface migration and desorption processes are ignored (generally true for low-temperature CVD processes such as PECVD), while hopping of *A* type macromolecules is allowed (as if *A* is firstly physisorbed). Surface reactions are not explicitly considered in this process, however, the long-range behavior of *A* and the surface relaxation of *B* could be consequences of surface reactions (i.e., surface mediated).

2.1. Microprocess model

The growth microprocess model is constructed based on a standard kMC scheme (Gillespie, 1976) which assumes the growth process to be a Poisson process. Therefore, the dynamics of the deposition process are governed by the master equation which describes the evolution of probabilities of the surface being in specific microconfigurations. Monte-Carlo simulation is used to obtain realizations of this stochastic process which are consistent with the master equation.

To simulate the heterogeneous deposition process studied in this work, a simple cubic lattice structure, which is a good approximation for amorphous films, is used. The simulated surface domain is a square grid of 100 lattice points by 100 lattice points. To improve computational efficiency, the solid-on-solid assumption is made (i.e., voids and overhangs are neglected). We consider a multi-layer growth and assume that all the sites are available for adsorption of all gas phase species at all times, and, thus, the adsorption rates of *A* (w_a^A) and *B* (w_a^B) are taken to be site independent; they can be obtained in real-time as discussed above.

To incorporate different growth behaviors into a kMC scheme, a viable way is to set up specific rules for the microprocesses considered in the scheme (see Shi et al. (2004) for an example of rule-based modelling of coating microstructure). Although, such rules may be arbitrary and may sacrifice the fidelity of the model with respect to the detailed physics and chemistry, they are very favorable from a computational point of view, and thus, preferable for real-time applications. Furthermore, when mechanisms of such behaviors are unknown, which is true for most of the complex PECVD processes, rule-based modelling must be used. In this work, we set up two rules for aggregation of *A* type macromolecule and surface relaxation of *B* type macromolecule, respectively.

For *A* type macromolecules, we enforce a rule on the hopping process. To encourage the aggregation of surface *A* macromolecules over long-range, we select the hopping direction of an *A* type macromolecule based on the number of the surface *A*s that the hopping *A* can see in each direction instead of randomly picking among the possible hopping directions. Specifically, the hopping direction of a specific *A* macromolecule is determined by comparing the distance-weighted sum of all the *A* macromolecules in each direction and pick the one with largest value of the sum. The weighted sum, for example, in the positive *x* direction of an *A* located at the surface lattice point (x_0, y_0), $N^A_{h,+x}(x_0, y_0)$, is computed as follows:

$$N^A_{h,+x}(x_0, y_0) = \sum_{x=1}^{l_a} \sum_{y=-x}^{x} S^A_{(x_0+x, y_0+y)} \times \left(1 - \frac{\sqrt{x^2+y^2}}{l_a}\right), \quad (1)$$

where l_a is the maximum range of attraction, and the value of the occupancy factor $S^A_{(i,j)}$ is unity when the surface site (i, j) is occupied by an *A* and zero otherwise. Eq. (1) imitates the sight of a surface *A* which fades out with distance, i.e., the near neighbors are weighted more than the distant neighbors. $1-\sqrt{x^2+y^2}/l_a$ is picked as the weighting function to employ a linearly decaying weighting which goes to zero at the boundary of the attraction zone, however, one can use any meaningful weighting function here to carry out simulations to simulate or validate specific deposition mechanisms.

The rate of the surface hopping of an *A* type macromolecule depends on the local activation energy barrier. Considering only the interactions of the first nearest side neighbors and the first nearest bottom neighbor to determine the hopping rate at a specific site, the hopping rate of a macromolecule of type *A* on the surface with *n* first nearest

side neighbors is given by

$$w_h^A(n) = k_{h0}^A \exp\left(-\frac{E_s^A + nE_n^A}{kT}\right), \quad (2)$$

where k_{h0}^A is the hopping frequency constant, E_s^A and E_n^A are the energy barriers associated with surface hopping of A for bottom and side neighbors, respectively (we note that for simplicity we do not distinguish the neighboring macromolecules of different types).

For B type macromolecules, we enforce a surface relaxation rule on the adsorption process. During an adsorption event, a site, (i, j), is first randomly picked among the sites of the whole lattice; the final site in which the B macromolecule adsorbs onto could be different from the initially chosen site for the adsorption event. In particular, when the initially chosen site does not have the local minimum height, B will be adsorbed onto one of the neighboring sites that has the local minimum height. In this work, only the 4 first nearest neighbor sites and 4 second nearest neighbor sites are considered. In addition, the sticking probability of type B macromolecule on surface site occupied by type A macromolecules is considered very small (5% in this study). This is because when this sticking probability is close to unity, the surface would be smoothened by type B macromolecules independently of the presence of type A macromolecules, and thus, the dynamics of the two-component deposition would not be observable. All other sticking probabilities are considered to be unity for simplicity.

The life time of each Monte-Carlo event in the simulation τ can be determined by the following expression (see Gillespie (1976) for a detailed proof):

$$\tau = -\frac{\ln \xi}{w_a^A + w_a^B + \sum_{n=0}^{4} N_n^A w_h^A(n)}, \quad (3)$$

where ξ is a random number that follows the uniform distribution in the unit interval and N_n^A is the number of A type macromolecules on the surface with n first nearest side neighbors.

Remark 1. Since we treat hopping events towards different hopping directions as different microscopic events, the kMC simulation does not need to determine which hopping direction the macromolecule needs to go once the event is selected, and therefore, overriding the direction chosen by kMC by the microprocess rule is not an issue here, and the time increment can be calculated using Eq. (3). Hopping processes towards different hopping directions are treated as independent Poisson processes just like the adsorption of A and the adsorption of B. As long as the dynamical hierarchy of transition rates is preserved in the kinetic Monte-Carlo simulation, the time increment should be selected from the exponential distribution of Eq. (3).

Table 1
Model parameters

Hopping freq. const.	k_{h0}^A	10^{13}	s^{-1}
Hopping energy (bottom)	E_s^A	0.8	eV
Hopping energy (side)	E_n^A	0.2	eV
Attraction range	l_a	20	Units

2.2. Simulation procedure

The parameters, k_{h0}^A, E_s^A, E_n^A and l_a in the model can be determined by optimal parameter estimation using experimental data, however, the parameters used in this study are arbitrarily chosen and are shown in Table 1. When the lattice is set and the rates of the three events (A adsorption, B adsorption, A hopping) are determined based on measurements or its corresponding rate expression (Eq. (2)), a kinetic Monte-Carlo simulation is executed following the algorithm reported in Vlachos (1997). First, the surface A macromolecules are grouped into five classes based on the number of side neighbors (from 0 to 4 side neighbors); in each class, the macromolecules have the same hopping rates, however, they may have different hopping directions depending on the surface microconfiguration; the adsorption rates of the A and B macromolecules are both site independent. Then, a random number is generated to select an event to be run based on the rates; if the event is A hopping, the class in which the event will happen is also selected. After that, a second random number is generated to select the site where the event will be executed; if the event is A or B adsorption, the site is randomly picked from sites in the entire lattice; if the event is A hopping, the site is randomly picked from the list of the sites in the selected class. After the site is selected, the MC event is executed. If the event is adsorption, it is executed by adding one macromolecule on the selected site (B adsorption rule is applied if the event is B adsorption); if the event is A hopping, the A type macromolecule on the site is moved to the next site in the direction selected by the hopping rule. Upon an executed event, a time increment τ computed based on Eq. (3) is added to the process time t. Periodic boundary conditions are used in the simulation to satisfy the mass balance of the hopping macromolecules.

Referring to the kMC simulation of the surface evolution using the microscopic process rules defined in subsection 2.1, it is important to note that we treat the surface evolution as a sequence of Poisson processes. Under this assumption, the evolution of the probability that the process (surface) is at a certain microscopic configuration σ at time t is determined by the so-called master equation:

$$\frac{\partial P(\sigma, t)}{\partial t} = \sum_{\sigma'} W(\sigma' \to \sigma) P(\sigma', t') - \sum_{\sigma'} W(\sigma \to \sigma') P(\sigma, t), \quad (4)$$

where σ and σ' are successive states of the system, $P(\sigma, t)$ is the probability that the system is in state σ at time t, and $W(\sigma' \to \sigma)$ is the probability per unit time that the system will undergo a transition from state σ' to σ. When the process reaches equilibrium (i.e., $\partial P(\sigma, t)/\partial t = 0$), this equation reduces to the so-called detailed-balance criterion:

$$\sum_{\sigma'} W(\sigma' \to \sigma) P(\sigma', t') = \sum_{\sigma'} W(\sigma \to \sigma') P(\sigma, t). \quad (5)$$

From Eqs. (4) and (5), it follows that during the dynamical evolution of the process (i.e., $\partial P(\sigma, t)/\partial t \neq 0$), the detailed balance should not be satisfied. Moreover, the strict detailed-balance criterion ($W(\sigma' \to \sigma) P(\sigma', \text{eq}) = W(\sigma \to \sigma') P(\sigma, \text{eq})$) does not even need to be satisfied at process equilibrium.

However, to correctly simulate the dynamical phenomena of a Poisson process, regardless of the existence of a process equilibrium, one needs to guarantee that the transition probabilities reflect unique transition rates. These probabilities should be formulated so that a dynamical hierarchy of transition rates is established in terms of appropriate models for the rates of the microscopic events considered in the entire process. To achieve such dynamical hierarchy for our process (which does not reach equilibrium), we choose the transition probability to be the rate of a specific event (e.g., the rate of a hopping event in a specific direction), divided by the sum of all the rates of the microscopic events. As we describe in the manuscript, we first choose a microscopic event among all possible adsorption events (A and B) and hopping events (A only, including hopping to all directions) based on the transition probabilities of adsorption and hopping; then, in the case of a hopping event, we choose a class of hopping events among all classes (each class includes hopping events towards different directions); once the class of the hopping event is selected, a hopping event of a specific macromolecule is randomly picked, since there are macromolecules with different hopping directions in each hopping class, the probability of picking a macromolecule hopping to the $+x$ direction should be $N^A_{n,+x}/N^A_n$ (where $N^A_{n,+x}$ is the number of surface macromolecules which have n nearest neighbors and hop towards the $+x$ direction once they are selected to hop). Therefore, the transition probability of a hopping event of an n nearest-neighbor surface macromolecule towards the $+x$ direction to occur can be computed as follows:

$$W_{h,+x}(n) = \frac{N^A_n w^A_h(n)}{w^A_a + w^B_a + \sum_{n=0}^{4} N^A_n w^A_h(n)} \times \frac{N^A_{n,+x}}{N^A_n} = \frac{N^A_{n,+x} w^A_h(n)}{w^A_a + w^B_a + \sum_{n=0}^{4} (N^A_{n,+x} + N^A_{n,-x} + N^A_{n,+y} + N^A_{n,-y}) w^A_h(n)}, \quad (6)$$

where $N^A_{n,-x}$, $N^A_{n,+y}$ and $N^A_{n,+y}$ are the number of surface macromolecules which have n nearest neighbors and hop towards the $-x$, $+y$ and $-y$ directions once they are selected to hop, respectively. We can see that the transition probability $W_{h,+x}$ is picked as the ratio of the rate of the $+x$ hopping event $N^A_{n,+x} w^A_h(n)$ over the sum of the rates of all microscopic events, and therefore, the transition probability is uniquely specified by the rate of the hopping event.

Moreover, if we were to study a process that would reach equilibrium, then the microscopic process rules should have been defined in a way such that the process is able to reach equilibrium, and accordingly, the detailed balance of the transition probabilities should have been satisfied at equilibrium. When the transition probabilities are formulated in the same way as we described above for a set of microscopic rules that constitute a process which goes to equilibrium, a dynamical hierarchy is achieved and the detailed balance criterion will be satisfied when the process reaches equilibrium.

3. Simulation results and discussion

Using the proposed growth model, a parametric analysis of the growth process is conducted. We study the effects of substrate temperature (in the range of 300–440 K, which is the normal operating temperature of low-temperature CVD processes such as PECVD) and gas phase composition on the surface microstructure of the deposited thin films in both homogeneous and heterogeneous deposition processes. Furthermore, the effect of simulation lattice size has also been investigated. This study provides valuable insight for the formulation of the control problem.

Island sizes of the thin films obtained under different process conditions are qualitatively compared and the surface roughness of each film, r, is computed in a root-mean-square fashion by the following expression:

$$r = \sqrt{\frac{\sum_{i=0}^{N} \sum_{j=0}^{N} (h_{ij} - \bar{h})^2}{N \times N}}, \quad (7)$$

where N is the size of the lattice, $\bar{h}$ is the average height of the film and h_{ij} is the height of the surface at position (i, j).

3.1. Single-component case

The simulation of a single component deposition process can be executed by setting either parameter w^A_a or w^B_a in the heterogeneous model equal to 0.

Fig. 2 shows the surface morphology of a thin film obtained by a deposition with only B type macromolecules present in the gas phase. It can be seen that the surface of the thin film is very smooth due to the surface

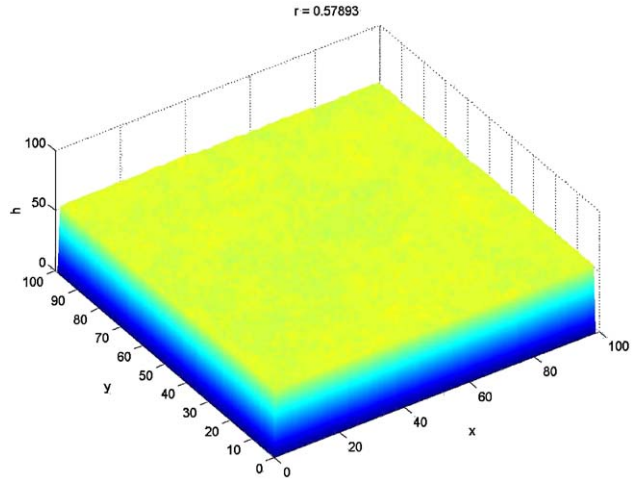

Fig. 2. Surface of a thin film deposited with $w_a^A = 0\,s^{-1}$, $w_a^B = 0.1\,s^{-1}$ and $T = 400\,K$ – $t = 550\,s$.

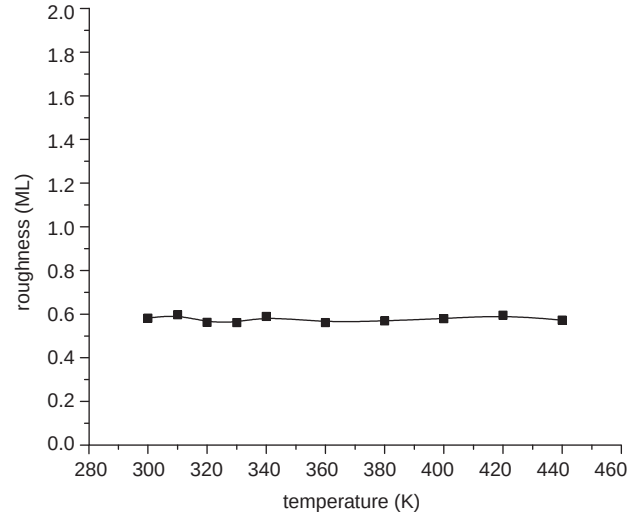

Fig. 3. Surface roughness of thin films deposited with $w_a^A = 0\,s^{-1}$, $w_a^B = 0.1\,s^{-1}$ for different substrate temperature – $t = 550\,s$.

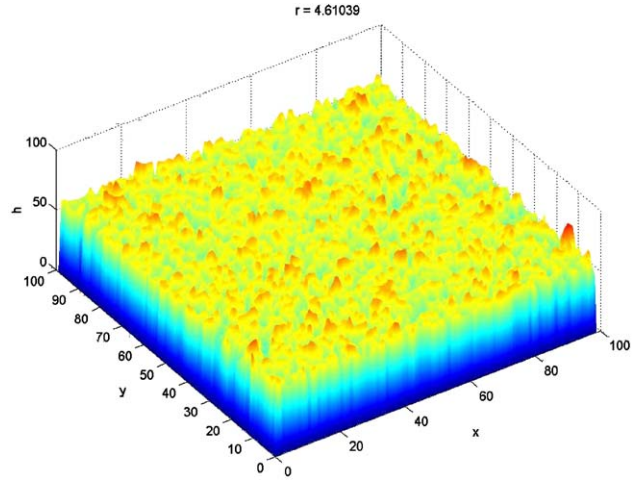

Fig. 4. Surface of a thin film deposited with $w_a^A = 0.1\,s^{-1}$, $w_a^B = 0\,s^{-1}$ and $T = 320\,K$ – $t = 570\,s$.

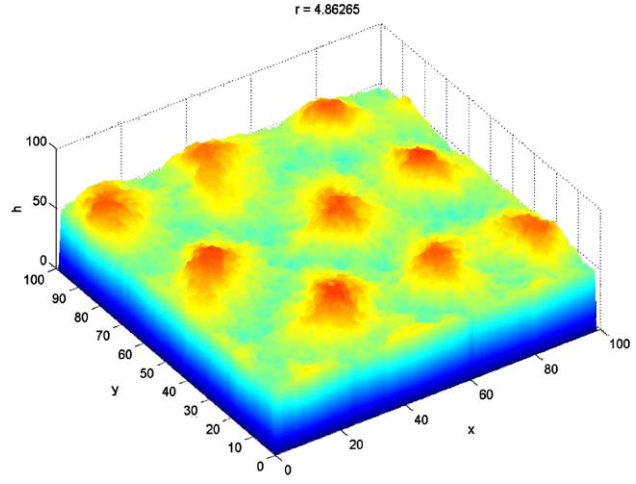

Fig. 5. Surface of a thin film deposited with $w_a^A = 0.1\,s^{-1}$, $w_a^B = 0\,s^{-1}$ and $T = 380\,K$ – $t = 570\,s$.

relaxation of *B*, and the film growth is in FM mode (see Fig. 7 (solid line) for the profile of the surface roughness during the deposition). Since the adsorption rate is independent of the substrate temperature, the surface microstructure of the thin film has no dependence on substrate temperature (Fig. 3).

Figs. 4 and 5 show the surface morphologies of thin films obtained by depositions with only *A* type macromolecules present in the gas phase at low and high substrate temperatures, respectively. The thin film deposited at low substrate temperature ($T = 320\,K$) has a high island density but a small lateral island size. The thin film deposited at high substrate temperature ($T = 380\,K$) has a low island density but a large lateral island size.

The very different surface microstructure observed for these two films, which have similar roughness values, can be explained by the different growth modes in these two temperature regimes. According to the hopping rate equation (Eq. (2)), surface hopping of *A* type macromolecules has an Arrhenius type dependence on substrate temperature *T*. Thus, at low substrate temperature, the hopping rate is much smaller than the rate at high substrate temperature. This suggests that at low temperature, the dominant surface microprocess is the adsorption process, therefore, although the long-range attraction tends to drive the surface *A* type macromolecules together, the hopping rate is so low that these macromolecules are not able to move along the direction of attraction far enough to form large islands. Therefore, the effect of long-range attraction is not significant and the aggregation mostly occurs in the vertical direction (one-dimensional (1D) aggregation) by *A* adsorption. This growth mechanism results in a surface with islands of large height and small lateral size.

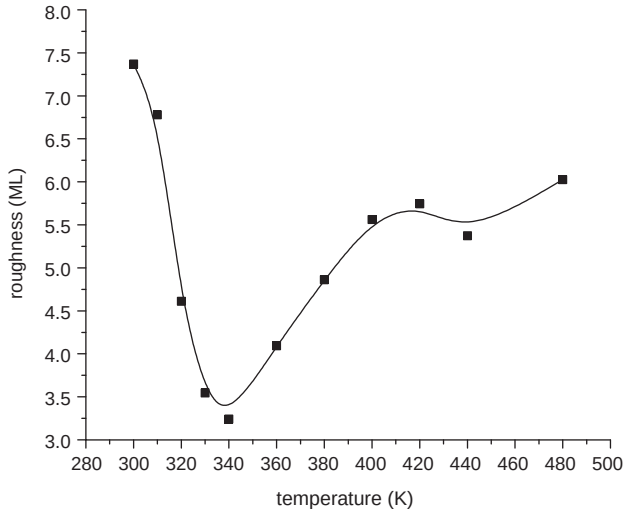

Fig. 6. Surface roughness of thin films deposited with $w_a^A = 0.1\,s^{-1}$, $w_a^B = 0\,s^{-1}$ for different substrate temperature – $t = 570\,s$.

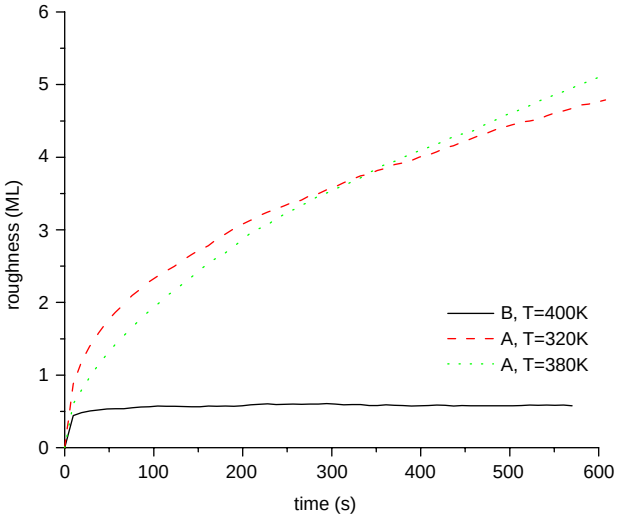

Fig. 7. Surface roughness of thin films during depositions with (a) $w_a^A = 0\,s^{-1}$, $w_a^B = 0.1\,s^{-1}$ and $T = 400\,K$ (solid line); (b) $w_a^A = 0.1\,s^{-1}$, $w_a^B = 0\,s^{-1}$ and $T = 320\,K$ (dashed line); (c) $w_a^A = 0.1\,s^{-1}$, $w_a^B = 0\,s^{-1}$ and $T = 380\,K$ (dotted line).

On the other hand, when the substrate temperature is high, the rate of hopping becomes large, surface *A* type macromolecules are able to move along the direction of attraction for a distance comparable to the range of attraction. Therefore, the effect of long-range attraction becomes very significant and aggregation occurs in both vertical and horizontal direction (3D aggregation, i.e., VW growth mode) by adsorption and hopping. This growth mechanism leads to the formation of islands with large dimensions in both the vertical and the horizontal directions. Furthermore, we note that although the range of attraction is limited to l_a, the lateral size of the islands are not limited by the range of interaction due to the coalescence between islands. Islands of lateral size larger than l_a are observed in our simulations for high substrate temperature depositions.

Fig. 6 shows the surface roughness of thin films deposited at different substrate temperatures. It can be clearly seen that there are two temperature regimes in which thin film growth is quite different. In the low-temperature regime, the surface roughness drops with increasing temperature, in the high-temperature regime, the surface roughness rises with increasing temperature (however, the surface roughness drops again when the substrate temperature is very high when stable surface islands start to coalesce and form islands with lateral dimension larger than the range of attraction). Based on the discussion above about the different growth modes at low and high substrate temperatures, the transition from the low-temperature regime to the high-temperature regime corresponds to the change in growth process from short-range interaction dominant to long-range attraction dominant. The substrate temperature at which the minimum roughness is achieved corresponds to the separation of the two temperature regimes.

Fig. 7 shows the profiles of the thin film surface roughness during the deposition. It can be clearly seen that the thin film

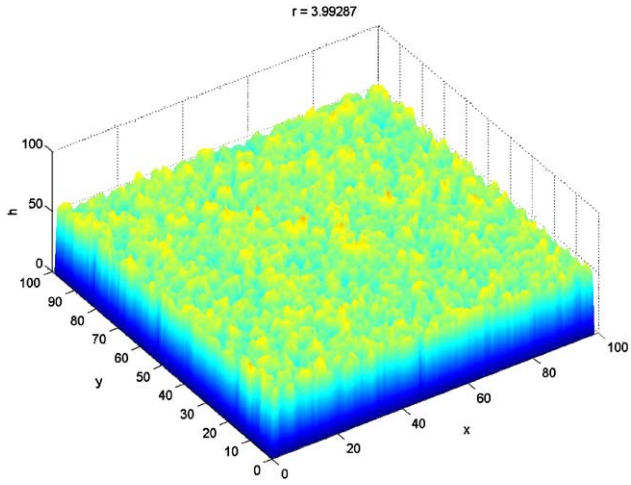

Fig. 8. Surface of a thin film deposited with $w_a^A = 0.05\,s^{-1}$, $w_a^B = 0.05\,s^{-1}$ and $T = 320\,K$ – $t = 900\,s$.

growth in the *B* only deposition is 2D growth (the surface roughness saturates over time) while the growth in the *A* only deposition, with either low or high substrate temperature, is 3D growth (the surface roughness never saturates).

3.2. Multi-component case

We have also simulated multi-component deposition which is heterogeneous, using the proposed process model. Both *A* and *B* types of macromolecules are present in the gas phase and the relative ratio of the two species is set to be unity in the simulated case for simplicity.

Figs. 8 and 9 show the surface morphology of thin films obtained by depositions at low ($T = 320\,K$) and high ($T =$

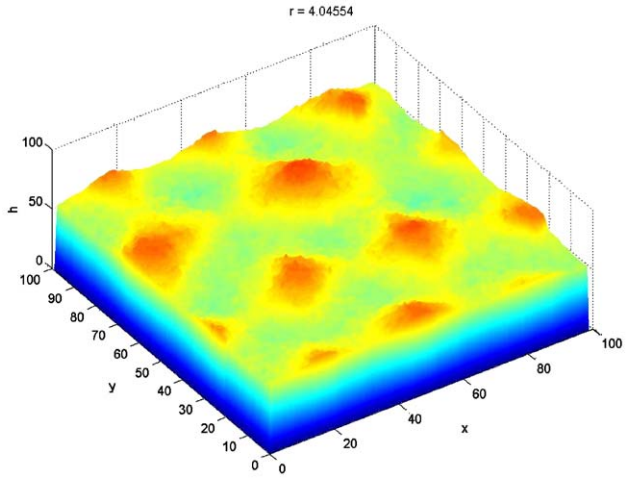

Fig. 9. Surface of a thin film deposited with $w_a^A = 0.05\,s^{-1}$, $w_a^B = 0.05\,s^{-1}$ and $T = 440\,K$ – $t = 900\,s$.

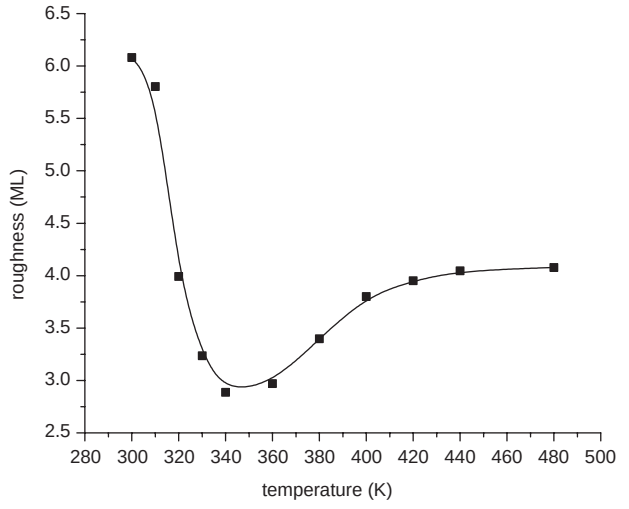

Fig. 10. Surface roughness of thin films deposited with $w_a^A = 0.05\,s^{-1}$, $w_a^B = 0.05\,s^{-1}$ for different substrate temperature – $t = 900\,s$.

440 K) substrate temperatures, respectively. The difference in surface morphology between the two thin films is similar to the single component case in which only *A* type macromolecules are present in the gas phase. This is expected since the behavior of the two types of macromolecules is considered independent of each other in the simulation.

Fig. 10 shows the surface roughness of thin films deposited at different substrate temperatures. Two temperature regimes can also be observed in the multi-component case, however, the absolute surface roughness values of the high substrate temperature regime are relatively small. To effectively compare the temperature dependence of surface roughness between homogeneous and heterogeneous processes, roughness values are plotted in Fig. 11 versus hopping to adsorption ratio (the ratio of the total number of hopping events to the total number of adsorption events in the

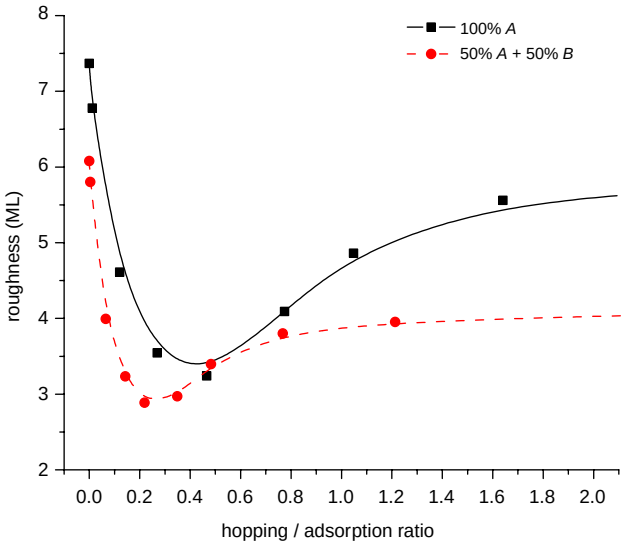

Fig. 11. Surface roughness of the thin films deposited for different hopping to adsorption ratio in (a) homogeneous deposition, 100%*A* (solid line); (b) heterogeneous deposition, 50%*A* + 50%*B* (dashed line).

overall simulation time), since the adsorption and the hopping events directly shape the surface of the thin films. In addition, this ratio of hopping to adsorption monotonically increases with increasing substrate temperature. It can be seen in Fig. 11 that a lower roughness value is observed for the heterogenous deposition compared to the homogeneous deposition. Furthermore, we note that the presence of *B* type macromolecules does affect the transition of the growth process from the short-range interaction dominant regime (low substrate temperature) to the long-range interaction dominant regime since the value of hopping to adsorption ratio that separates the two regimes of the multi-component case is smaller than that of the single-component case. This may be due to the fact that the presence of *B* type macromolecules in the gas phase facilitates the smoothening of the film surface by adsorbing onto surface sites with local minimum heights. However, in both cases the dependence of surface roughness on substrate temperature is almost the same; this observation suggests that the temperature dependence of the heterogeneous deposition is qualitatively determined by *A* type macromolecules.

3.3. Effect of gas phase composition

Since different gas phase compositions can be used to tailor the material properties of the thin films obtained by the depositions for different applications, simulations of depositions for different gas phase compositions have been run to study the effect of gas phase composition on the surface microstructure based on the proposed growth model. We note that since the adsorption of type *B* macromolecule is surface site-dependent, the growth rate of the thin film varies with gas phase composition. Therefore, compari-

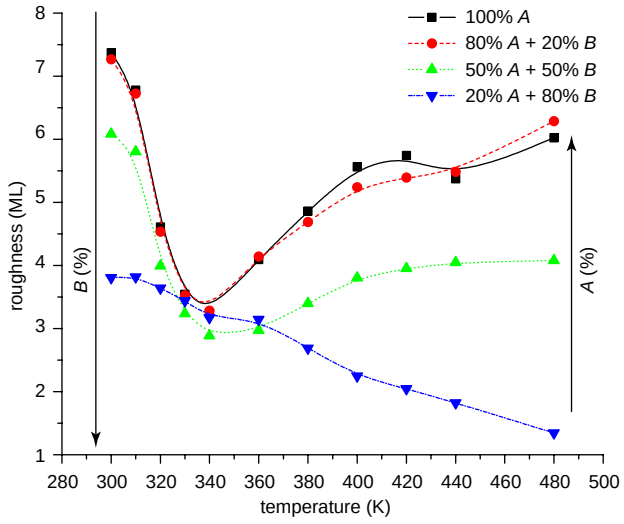

Fig. 12. Surface roughness of thin films deposited with different gas phase compositions: (a) 100%A (solid line); (b) 80%$A + 20\%B$ (dashed line); (c) 50%$A + 50\%B$ (dotted line); (d) 20%$A + 80\%B$ (dashed dotted line).

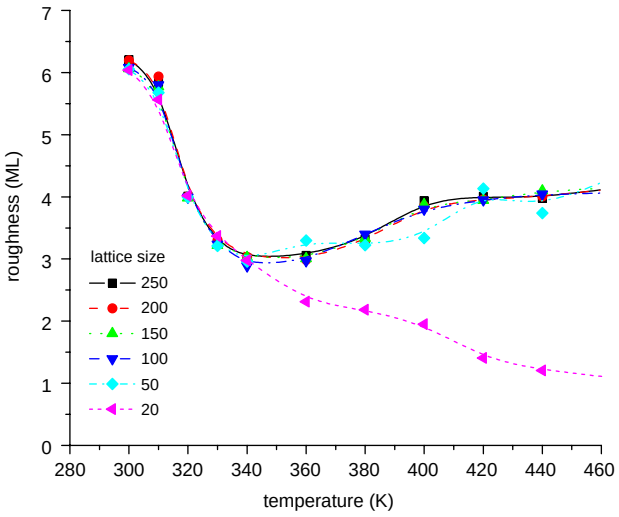

Fig. 13. Surface roughness of thin films deposited with different substrate temperature computed using different simulation lattice size.

son has been conducted between thin films with the same thickness.

Fig. 12 shows the surface roughness of thin films deposited for different gas phase compositions. It can be seen that the increase of relative concentration of A leads to increasing surface roughness and vice versa. Moreover, when the relative concentration of A is larger than 50%, the presence of two temperature regimes is quite clear. This again suggests that type A macromolecules have significant effect on the surface microstructure when the relative concentrations of A and B are comparable.

3.4. Effect of lattice size

Because the dimension of the wafers used in a real deposition process is usually in the 10^8 nm regime, it is impossible to simulate the film growth for the entire wafer even with the most efficient Monte-Carlo algorithm and the best available computing power, and thus, a lattice size which corresponds to a very small spatial domain compared to the actual wafer dimension is used in this work. However, to better gauge the results from such simulations, investigating the lattice size dependency of the simulation results is necessary.

Fig. 13 shows the surface roughness of thin films deposited with different substrate temperature computed using different simulation lattice size. It can be seen that simulation results from kMC runs with lattice size larger than 50×50 agree very well with each other, while simulation results from the 50×50 lattice show qualitative agreement with the results from the larger lattice runs. However, the result from the 20×20 lattice is inconsistent with all other results. Such results suggest that the lattice size used in the kMC simulation should be at least twice as large as the surface interaction radius (20 in this work) to capture the dynamics of the thin film growth process. Moreover, the stochastic noise of the simulation decreases with increasing lattice size. For this work in particular, simulation lattice size of 100×100 is large enough to describe the process dynamics with low stochastic noise, and therefore, such a lattice size (or larger) will be used in the subsequent simulations.

4. Feedback control

To obtain thin films of desired and reproducible surface microstructure, it is necessary to operate the deposition process under feedback control. In this process, since there are two temperature regimes for which thin film surface morphologies are quite different, control of surface roughness in these two regimes is considered separately.

The final surface roughness of the thin film is selected as the controlled variable because this is the quantity of interest from a practical point of view. The manipulated variable is chosen to be the substrate temperature T, since, in low-temperature CVD processes, such as PECVD, the substrate temperature is usually one of the few process variables that could be allowed to vary in practice. Moreover, the manipulation of substrate temperature is relatively easy and has been integrated on most deposition systems. The major disturbance to the deposition process is the variation of the gas phase composition. Such variation may be caused by gas flow spikes in the gas delivery system.

4.1. Surface roughness control in the low-temperature regime

For thin film applications where high island density is desired, surface roughness control can be implemented on the low-temperature regime, in which the growth process is dominated by short-range interactions. Real-time feedback

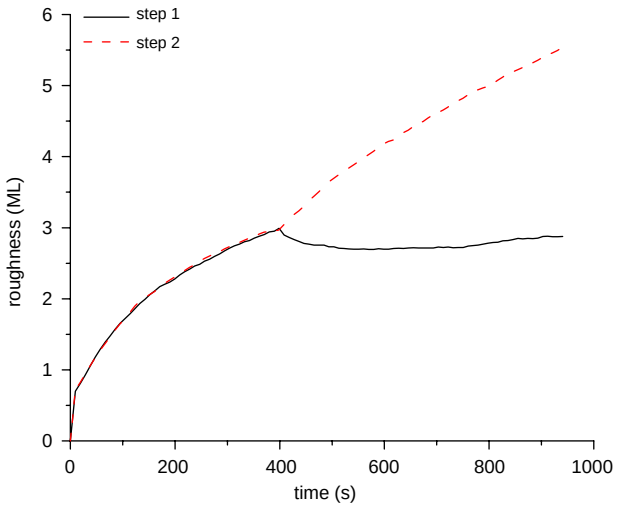

Fig. 14. Response of surface roughness with respect to step changes in substrate temperature: (a) T changes from 320 to 340 K at $t = 400$ s (step 1); (b) T changes from 320 to 300 K at $t = 400$ s (step 2).

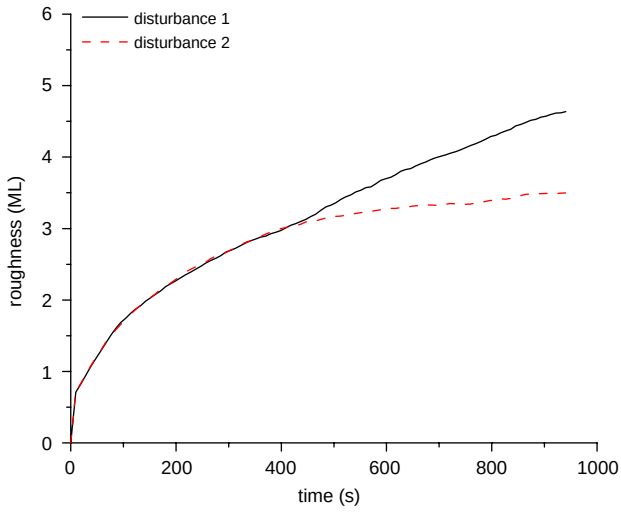

Fig. 15. Response of surface roughness with respect to step disturbance in gas phase composition: (a) gas phase composition changed from $50\%A + 50\%B$ to $70\%A + 30\%B$ (disturbance 1); (b) gas phase composition changed from $50\%A + 50\%B$ to $30\%A + 70\%B$ (disturbance 2).

control of deposition processes which are characterized by short-range interactions has been discussed in detail by Lou and Christofides (2003a,b), where the control problem was formulated as regulation of instantaneous surface roughness. In this work, a feedback control scheme inspired by the methodology proposed by Lou and Christofides (2003a,b) is developed to regulate the final surface roughness. To ensure that the surface of the thin film has a high island density, the substrate temperature is restricted within the range of 300–340 K.

4.1.1. Open-loop response

Fig. 14 shows the response profiles of the surface roughness with respect to step changes (±20 K) in the substrate temperature at time $t = 400$ s. We can see that the value of the surface roughness at the end of the deposition can be controlled by manipulating the substrate temperature. The final surface roughness can be computed based on the current thin film surface, the gas flux composition and the substrate temperature using the proposed kMC growth model. In all simulation runs, the final surface roughness is considered to be the roughness at $t = 950$ s.

Fig. 15 shows the profiles of surface roughness with respect to disturbances in the gas phase composition (i.e., gas flux pattern). It can be seen that increasing concentration of A type macromolecules in the gas phase, i.e., increasing w_a^A, results in a rise in the final thin film surface roughness and vice versa. Therefore, feedback control is needed to reject such disturbances.

4.1.2. Controller design—closed-loop simulation

Based on the open-loop system analysis, a real-time surface roughness feedback control scheme is designed for the process. Fig. 16 shows the block diagram of the closed-loop system. The thin film growth is influenced by the substrate

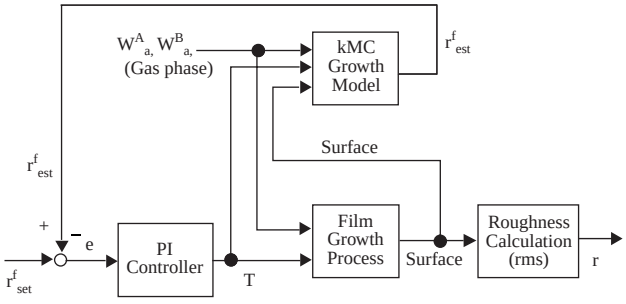

Fig. 16. Block diagram of the closed-loop system.

temperature and the macromolecule adsorption rates which are determined by gas phase composition. Since we choose the final surface roughness as the variable to control, an estimate is computed for every control cycle using the proposed kMC model based on the operating conditions and the thin film surface configuration which can be measured in real-time by advanced surface characterization tools such as the GISAXS (Renaud et al., 2003).

The substrate temperature, is then computed based on a proportional integral (PI) control algorithm as follows:

$$T(t) = K_c \hat{e}(t) + K_i \int_{t_0}^{t} \hat{e}(\mu)\, \mathrm{d}\mu + T_0, \tag{8}$$

$$\hat{e}(t) = \begin{cases} e(t) & |e(t)| > \varepsilon, \\ 0 & |e(t)| \leqslant \varepsilon, \end{cases} \tag{9}$$

where $T(t)$ is the controller output (i.e., substrate temperature), T_0 is the initial substrate temperature, K_c is the proportional gain, K_i is the integral gain, $e(t)$ is the error of the

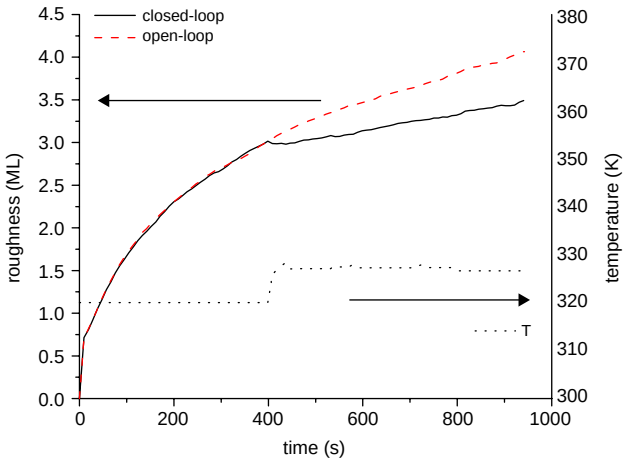

Fig. 17. Temperature and surface roughness profiles with surface roughness set-point value of 3.5 ML: (a) closed-loop surface roughness (solid line, left scale); (b) open-loop surface roughness (dashed line, left scale); (c) substrate temperature (dotted line, right scale).

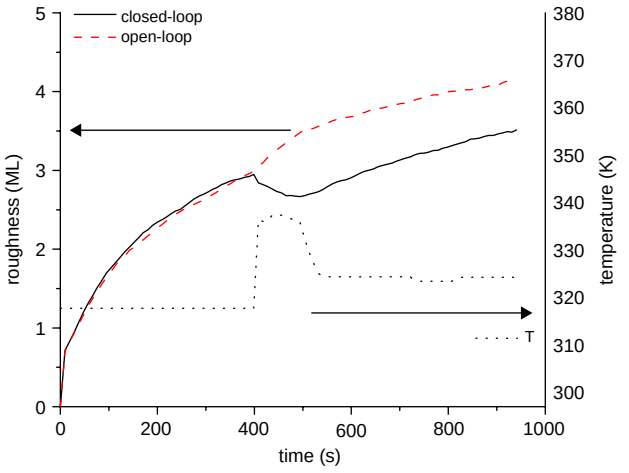

Fig. 18. Temperature and surface roughness profiles with surface roughness set-point value of 3.5 ML in the presence of disturbance: (a) closed-loop surface roughness (solid line, left scale); (b) open-loop surface roughness (dashed line, left scale); (c) substrate temperature (dotted line, right scale).

final surface roughness (i.e., the difference between the desired final surface roughness and the estimated final surface roughness computed using the proposed kMC model based on the surface configuration and operating conditions at the instance of last control action) and ε is the error tolerance ($\varepsilon = 0.05$ in this work).

The closed-loop thin film growth process which employs the proposed real-time feedback control scheme has been simulated. The controller parameters K_c and K_i are set to be -0.1 and -0.5, respectively. For all the closed-loop simulations, the deposition duration is set to be 950 s and the adsorption rates w_a^A and w_a^B are both set to be $0.05\,s^{-1}$. The estimator and controller are activated at $t = 400$ s and the control action is applied to the process every 10 s.

Fig. 17 shows the temperature and surface roughness profiles with final surface roughness set-point value of 3.5 ML. It can be seen that the surface roughness value of the thin film at the end of the deposition has been controlled at the desired value which is 12.5% lower than the surface roughness of the thin film deposited by open-loop deposition with the same initial deposition conditions.

Fig. 18 shows the temperature and surface roughness profiles with final surface roughness set-point value of 3.5 ML. A disturbance in the gas phase composition is introduced in this simulation represented by a step change in the adsorption rates at $t = 400$–500 s. Specifically, w_a^A changed from 0.05 to $0.1\,s^{-1}$ and w_a^B changed from 0.05 to $0\,s^{-1}$ at $t = 400$ s, while at $t = 500$ s, w_a^A and w_a^B both changed back to $0.05\,s^{-1}$. It can be seen that the surface roughness of the thin film at the end of the deposition has been controlled at the desired value in spite of the disturbance in the gas phase, while the thin film deposited by open-loop deposition has a surface roughness 19.2% higher than the desired value due to the disturbance.

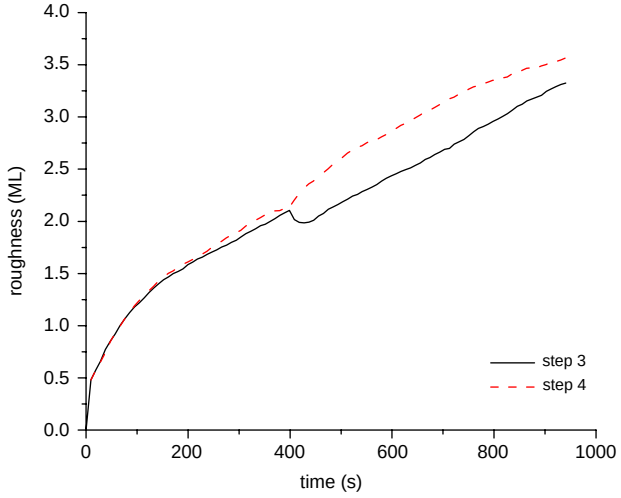

Fig. 19. Response of surface roughness with respect to step changes in substrate temperature: (a) T changes from 370 to 410 K at $t = 400$ s (step 3); (b) T changes from 370 to 330 K at $t = 400$ s (step 4).

4.2. Surface roughness control in the high-temperature regime

For thin film applications where large island size is desired, surface roughness control can be implemented for the high-temperature regime, in which the growth process is dominated by long-range interactions. To ensure the surface of the thin film has a low island density, the substrate temperature is restricted within the range of 340–420 K.

4.2.1. Open-loop response

Fig. 19 shows the response profiles of the surface roughness with respect to step changes (±40 K) in substrate temperature at time $t = 400$ s. We can see that, in the

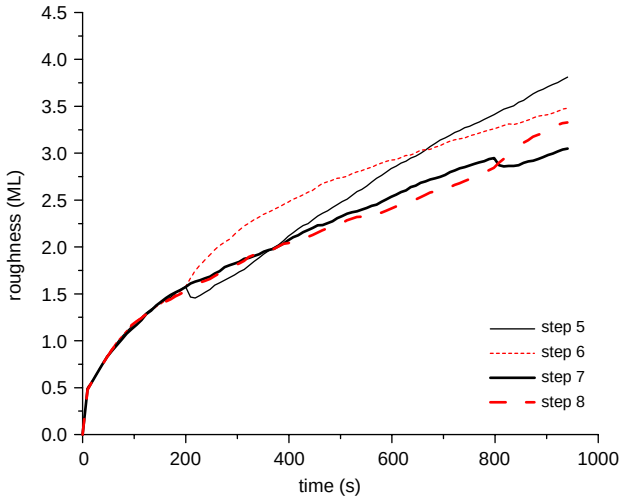

Fig. 20. Response of surface roughness with respect to step changes in substrate temperature: (a) T changes from 370 to 410 K at $t = 200$ s (step 5); (b) T changes from 370 to 330 K at $t = 200$ s (step 6); (c) T changes from 370 to 410 K at $t = 800$ s (step 7); (d) T changes from 370 to 330 K at $t = 800$ s (step 8).

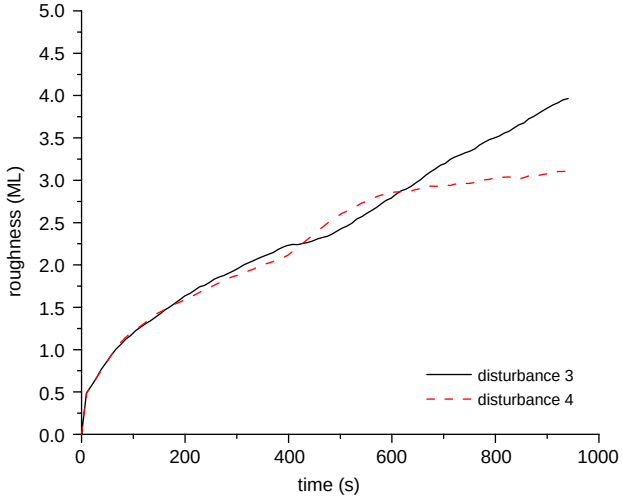

Fig. 21. Response of surface roughness with respect to step disturbance in gas phase composition: (a) gas phase composition changed from $50\%A + 50\%B$ to $80\%A + 20\%B$ (disturbance 3); (b) gas phase composition changed from $50\%A + 50\%B$ to $20\%A + 80\%B$ (disturbance 4).

high-temperature regime, the value of the surface roughness at the end of the deposition can also be controlled by manipulating the substrate temperature. However, the responses to step changes in substrate temperature exhibit inverse dynamics as shown in Fig. 20. This result suggests that a more advanced controller may be needed to control the surface roughness in the high-temperature regime. Fig. 21 shows the profiles of surface roughness with respect to disturbances in the gas phase composition (i.e., gas flux pattern). It can be seen that, in the high-temperature regime, the effect of disturbance in the gas phase composition on

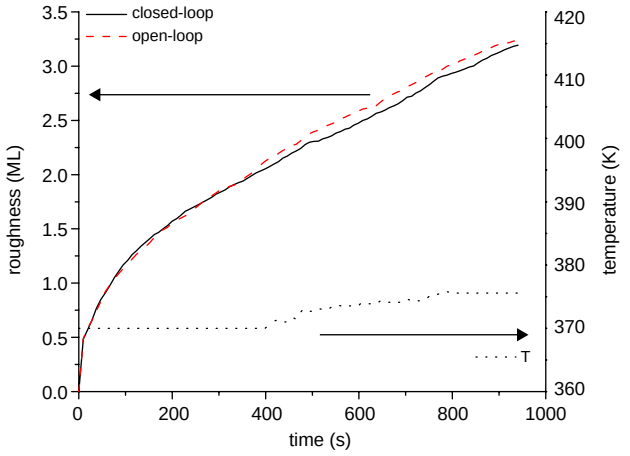

Fig. 22. Temperature and surface roughness profiles with surface roughness set-point value of 3.2 ML: (a) closed-loop surface roughness (solid line, left scale); (b) open-loop surface roughness (dashed line, left scale); (c) substrate temperature (dotted line, right scale).

the surface roughness also leads to inverse response, and thus, the proposed growth model is needed to predict the evolution of the surface roughness.

4.2.2. Controller design—PI control

The high-temperature regime closed-loop thin film growth process which employs the proposed real-time feedback control scheme for the low-temperature regime but with different controller parameters has been simulated. The controller parameters K_c and K_i are set to be -2 and -0.2, respectively.

Fig. 22 shows the temperature and surface roughness profiles with final surface roughness set-point value of 3.2 ML. It can be seen that the surface roughness value of the thin film at the end of the deposition has been controlled at the desired value which is about the same as the surface roughness of the thin film deposited by open-loop deposition with the same initial deposition conditions.

Fig. 23 shows the temperature and surface roughness profiles with final surface roughness set-point value of 3.2 ML. A disturbance in the gas phase composition is introduced in this simulation in terms of a step change in the adsorption rates at $t = 400$–420 s. Specifically, w_a^A changed from 0.05 to 0.1 s^{-1} and w_a^B changed from 0.05 to 0 s^{-1} at $t = 400$ s, while at t=420 s, w_a^A and w_a^B both changed back to 0.05 s^{-1}. It can be seen that the final surface roughness has been controlled at the desired value which is 5.9% lower than the one obtained under open-loop operation in spite of the disturbance in the gas phase.

Fig. 24 shows the temperature and surface roughness profiles with final surface roughness set-point value of 3.2 ML. A disturbance in the gas phase composition is introduced in this simulation in terms of a step change in the adsorption rates at $t = 400$–500 s. Specifically, at $t = 400$ s, w_a^A changed from 0.05 to 0.1 s^{-1} and w_a^B changed from 0.05 to 0 s^{-1},

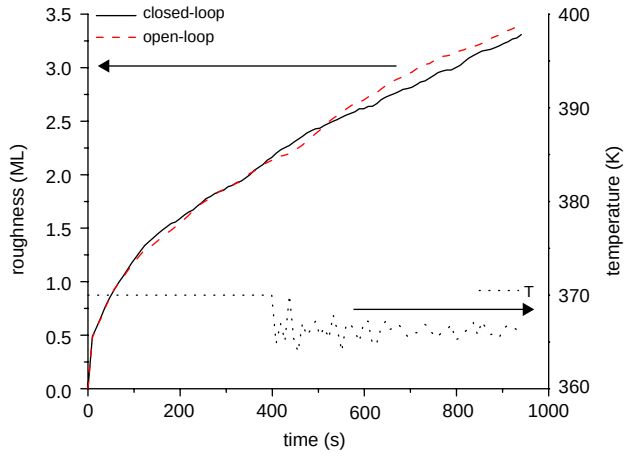

Fig. 23. Temperature and surface roughness profiles with surface roughness set-point value of 3.2 ML in the presence of disturbance: (a) closed-loop surface roughness (solid line, left scale); (b) open-loop surface roughness (dashed line, left scale); (c) substrate temperature (dotted line, right scale).

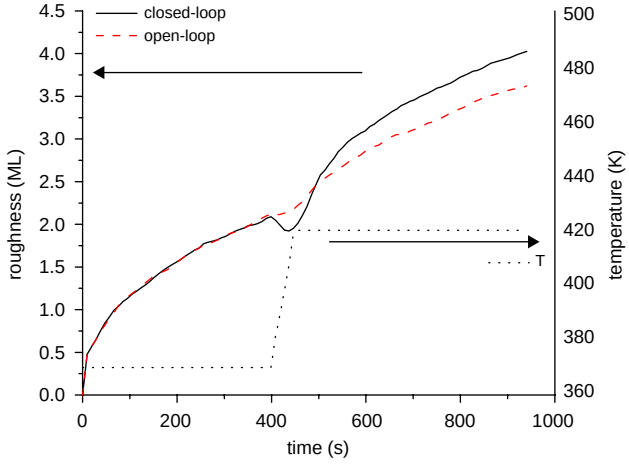

Fig. 24. Temperature and surface roughness profiles with surface roughness set-point value of 3.2 ML in the presence of disturbance: (a) closed-loop surface roughness (solid line, left scale); (b) open-loop surface roughness (dashed line, left scale); (c) substrate temperature (dotted line, right scale).

while at $t=500$ s, w_a^A and w_a^B both changed back to $0.05\,s^{-1}$. It can be seen that the surface roughness is not controlled at the desired value and that the controller output hits the high limit of the control actuator. The final surface roughness is about 13.9% higher than the one obtained under open-loop operation. This suggests that the kMC estimator-based PI controller does not provide satisfactory closed-loop performance when the disturbance to the process is significant, and therefore, a more advanced control scheme is needed.

4.2.3. Controller design—kMC model-based predictive control

In order to achieve robust closed-loop operation in the high-temperature regime, a kMC model-based predictive control scheme is proposed. Fig. 25 shows the block diagram of the closed-loop system. A reference trajectory of the instantaneous surface roughness of the thin film is selected based on off-line optimization, and in this work for simplicity, the profile of the surface roughness of the thin film in an ideal open-loop deposition (no disturbance is assumed to affect the process and the final surface roughness is taken to be the desired value) is chosen. Using such a reference trajectory, instead of solving the receding horizon optimization problem of minimizing the difference between the final surface roughness and the desired value with multiple decision variables, we only need to solve the fixed short horizon optimization problem of minimizing the difference between the instantaneous surface roughness and the reference value with a single decision variable. Therefore, the computation time of each optimization is greatly reduced, since the kMC simulation duration is reduced from the scale of the total deposition time to the controller turnover time. This is very important since kMC simulation is relatively time consuming and large scale numerical optimization using kMC models is almost impossible to solve in real-time.

During each control cycle, the surface configuration $X(k)$ (i.e., the height and the types of the top two macromolecules of each surface site) is first measured. An estimate of the surface configuration at the next control action time $X_{\mathrm{est}}(k+1)$ is computed based on the current process conditions using the proposed kMC model, and the estimated surface roughness value $r_{\mathrm{est}}(k+1)$ is compared with the reference value $r_{\mathrm{ref}}(k+1)$. If the error is less than ε ($\varepsilon=0.05$ in this work), the next controller output $T(k+1)$ is set to be the same as the current output $T(k)$. If the error is larger than ε, the optimizer is called to compute the output value of the next control action $T(k+1)$ so that the error between the surface roughness after the next control action $r(k+2)$ and the reference value $r_{\mathrm{ref}}(k+2)$ is minimized.

The optimizer uses direct search to find the optimal solution since the kMC model does not have a closed-form expression. The estimate of the surface roughness after the next control action $r_{\mathrm{est}}(k+1)$ is computed using the proposed kMC model based on the estimated surface configuration before the next control action $X_{\mathrm{est}}(k+1)$, the probe output value $T_{\mathrm{probe}}(k+1)$ and current process conditions. The search precision specified in this work is 1 K, and since the proposed kMC model is highly computationally efficient, the optimization problem can be solved by an entry level personal computer within the controller turnover time (10 s). Furthermore, the speed and the precision of the direct search optimization algorithm can be substantially improved by parallel computing.

Fig. 26 shows the temperature and surface roughness profiles with final surface roughness set-point value of 3.2 ML. The reference trajectory is computed by averaging the open-loop surface roughness profiles from six independent simulation runs. It can be seen that the surface roughness value of the thin film follows the reference trajectory closely and the final surface roughness has been controlled at the desired value.

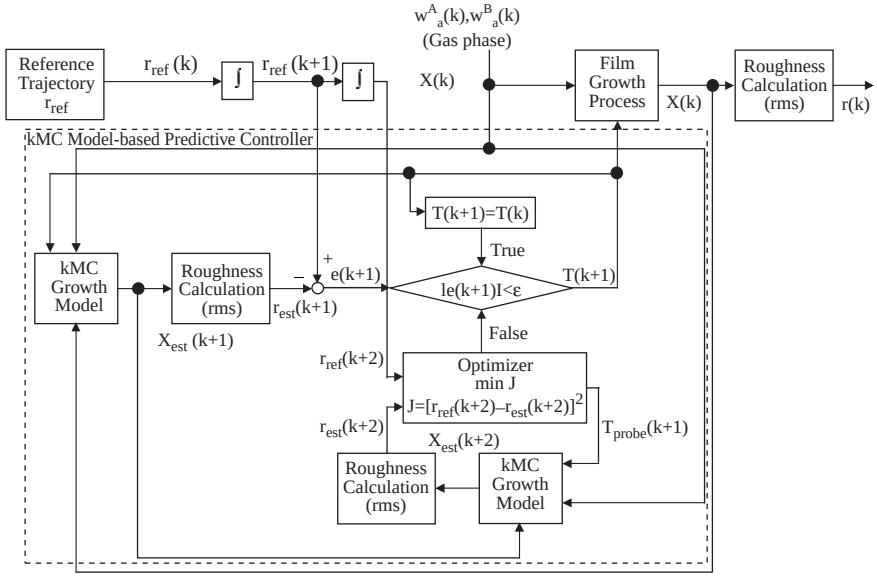

Fig. 25. Block diagram of the closed-loop system with the kMC model-predictive controller.

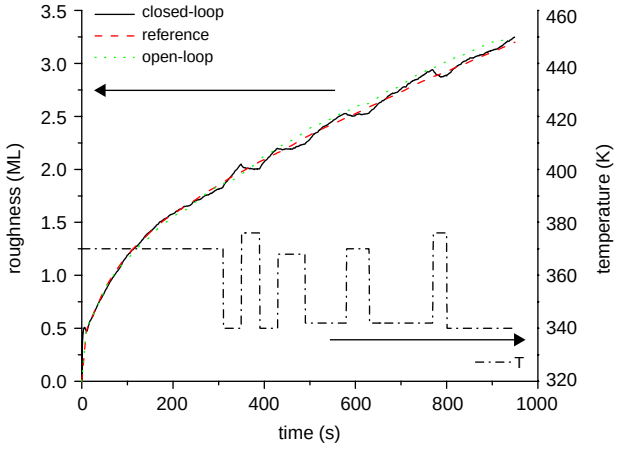

Fig. 26. Temperature and surface roughness profiles with surface roughness set-point value of 3.2 ML: (a) closed-loop surface roughness (solid line, left scale); (b) reference surface roughness (dashed line, left scale); (c) open-loop surface roughness (dotted line, left scale); (d) substrate temperature (dashed dotted line, right scale).

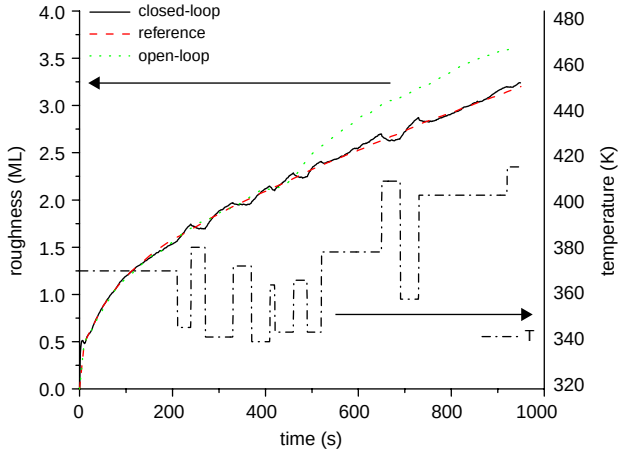

Fig. 27. Temperature and surface roughness profiles with surface roughness set-point value of 3.2 ML: (a) closed-loop surface roughness (solid line, left scale); (b) reference surface roughness (dashed line, left scale); (c) open-loop surface roughness (dotted line, left scale); (d) substrate temperature (dashed dotted line, right scale).

Fig. 27 shows the temperature and surface roughness profiles with final surface roughness set-point value of 3.2 ML. A disturbance in the gas phase composition is introduced in this simulation in terms of a change in the adsorption rates at $t = 400$–500 s. Specifically, w_a^A changed from 0.05 to 0.1 s^{-1} and w_a^B changed from 0.05 to 0 s^{-1} at $t = 400$ s, while at $t = 500$ s, w_a^A and w_a^B both changed back to 0.05 s^{-1}. It can be seen that the surface roughness follows closely the reference trajectory and the final surface roughness has been controlled at the desired value which is 13.5% lower than the open-loop value. Compared to the failure of the PI controller on the same closed-loop simulation case, the kMC model-based predictive controller delivers substantially improved and robust closed-loop performance.

5. Conclusions

In this work, a complex deposition process, which included two types of macromolecules whose growth behaviors were very different, was investigated. This deposition process was influenced by both short- and long-range interactions. A multi-component kMC model was developed for the deposition. Both single- and multi-component cases were simulated and the dependence of the surface mi-

crostructure of the thin film, such as island size and surface roughness, on substrate temperature and gas phase composition were studied. The surface morphology was found to be strongly influenced by these two factors and growth regimes governed by short- and long-range interactions were observed. Furthermore, two kMC model-based feedback control schemes which use the substrate temperature to control the final surface roughness of the thin film were proposed. The closed-loop simulation results demonstrated that robust deposition with controlled thin film surface roughness could be achieved under a kMC estimator-based PI feedback controller in the short-range interaction dominated growth regime, while a kMC model-predictive controller was needed to control the surface roughness in the long-range interaction dominated growth regime.

Acknowledgements

Financial support for this work from the NSF (ITR), CTS-0325246, is gratefully acknowledged.

References

Armaou, A., Christofides, P.D., 1999. Plasma-enhanced chemical vapor deposition: modeling and control. Chemical Engineering Science 54, 3305–3314.

Armaou, A., Siettos, C.I., Kevrekidis, I.G., 2004. Time-steppers and 'coarse' control of distributed microscopic processes. International Journal of Robust and Nonlinear Control 14, 89–111.

Baker, J., Christofides, P.D., 1999. Output feedback control of parabolic PDE systems with nonlinear spatial differential operators. Industrial and Engineering Chemistry Research 38, 4372–4380.

Battaile, C.C., Srolovitz, D.J., 2002. Kinetic Monte Carlo simulation of chemical vapor deposition. Annual Review of Materials Research 32, 297–319.

Cho, B., Wang, J., Chang, J.P., 2002. Metalorganic precursor decomposition and oxidation mechanisms in plasma-enhanced ZrO_2 deposition. Journal of Applied Physics 92 (8), 4238.

Cho, B., Chang, J.P., Min, J., Moon, S.H., Kim, Y.W., Levin, I., 2003. Material characteristics of electrically tunable zirconium oxide thin films. Journal of Applied Physics 93, 745–749.

Christofides, P.D., 2001. Nonlinear and Robust Control of Partial Differential Equation Systems: Methods and Applications to Transport-Reaction Processes. Birkhäuser, Boston.

Einstein, T.L., 1996. Handbook of Surface Science, vol. 1. Elsevier, Amsterdam, pp. 577–650 (Chapter 11).

Gallivan, M.A., Murray, R.M., 2004. Reduction and identification methods for Markovian control systems, with application to thin film deposition. International Journal of Robust and Nonlinear Control 14, 113–132.

Gillespie, D.T., 1976. A general method for numerically simulating the stochastic time evolution of coupled chemical reactions. Journal of Computational Physics 22, 403–434.

Gilmer, G.H., Huang, H., Roland, C., 1998. Thin film deposition: fundamentals and modeling. Computational Materials Science 12, 354–380.

Lam, R., Vlachos, D.G., 2001. Multiscale model for epitaxial growth of films: growth mode transition. Physical Review B 64, 035401.

Lou, Y., Christofides, P.D., 2003a. Estimation and control of surface roughness in thin film growth using kinetic Monte-Carlo models. Chemical Engineering Science 58, 3115–3129.

Lou, Y., Christofides, P.D., 2003b. Feedback control of growth rate and surface roughness in thin film growth. A.I.Ch.E. Journal 49, 2099–2113.

Lou, Y., Christofides, P.D., 2005a. Feedback control of surface roughness of GaAs (0 0 1) thin films using kinetic Monte-Carlo models. Computers and Chemical Engineering, 29, 225–241.

Lou, Y., Christofides, P.D., 2005b. Feedback control of surface roughness using stochastic PDEs. A.I.Ch.E. Journal, to appear.

Lou, Y., Christofides, P.D., 2005c. Feedback control of surface roughness in sputtering processes using the stochastic Kuramoto–Sivashinsky equation. Computers and Chemical Engineering, to appear.

Merrick, M.L., Luo, W., Fichthorn, K.A., 2003. Substrate-mediated interactions on solid surfaces: theory, experiment, and consequences for thin-film morphology. Progress in Surface Science 72, 117–134.

Ni, D., Christofides, P.D., 2005a. Construction of stochastic PDEs for feedback control of surface roughness in thin film deposition. International Journal of Robust and Nonlinear Control, submitted for publication.

Ni, D., Christofides, P.D., 2005b. Multivariable predictive control of thin film deposition using a stochastic PDE model. Industrial and Engineering Chemistry Research, in press.

Ni, D., Lou, Y., Christofides, P.D., Sha, L., Lao, S., Chang, J.P., 2004. Real-time carbon content control for PECVD ZrO_2 thin film growth. IEEE Transactions on Semiconductor Manufacturing 17, 221–230.

Reese, J.S., Raimondeau, S., Vlachos, D.G., 2001. Monte Carlo algorithms for complex surface reaction mechanisms: efficiency and accuracy. Journal of Computational Physics 173, 302–321.

Renaud, G., Lazzari, R., Revenant, C., Barbier, A., Noblet, M., Ulrich, O., Leroy, F., Jupille, J., Borensztein, Y., Henry, C.R., Deville, J.P., Scheurer, F., Mane-Mane, J., 2003. Real-time monitoring of growing nanoparticles. Science 300, 1416–1419.

Shi, D., Li, M., Christofides, P.D., 2004. Diamond jet hybrid HVOF thermal spray: rule-based modeling of coating microstructure. Industrial and Engineering Chemistry Research 43, 3653–3665.

Siettos, C.I., Armaou, A., Makeev, A.G., Kevrekidis, I.G., 2003. Microscopic/stochastic timesteppers and "coarse" control: a kMC example. A.I.Ch.E. Journal 49, 1922–1926.

Theodoropoulou, A., Adomaitis, R.A., Zafiriou, E., 1999. Inverse model based real-time control for temperature uniformity of RTCVD. IEEE Transactions on Semiconductor Manufacturing 12, 87–101.

Vlachos, D.G., 1997. Multiscale integration hybrid algorithms for homogeneous–heterogeneous reactors. A.I.Ch.E. Journal 43, 3031–3041.